Brian F. Zamarron,[1] Taleen A. Mergian,[2] Kae Won Cho,[3]
Gabriel Martinez-Santibanez,[4] Danny Luan,[2] Kanakadurga Singer,[1,5]
Jennifer L. DelProposto,[5] Lynn M. Geletka,[5] Lindsey A. Muir,[5] and
Carey N. Lumeng[1,4,5]

Macrophage Proliferation Sustains Adipose Tissue Inflammation in Formerly Obese Mice

OBESITY STUDIES

Obesity causes dramatic proinflammatory changes in the adipose tissue immune environment, but relatively little is known regarding how this inflammation responds to weight loss (WL). To understand the mechanisms by which meta-inflammation resolves during WL, we examined adipose tissue leukocytes in mice after withdrawal of a high-fat diet. After 8 weeks of WL, mice achieved similar weights and glucose tolerance values as age-matched lean controls but showed abnormal insulin tolerance. Despite fat mass normalization, total and CD11c$^+$ adipose tissue macrophage (ATM) content remained elevated in WL mice for up to 6 months and was associated with persistent fibrosis in adipose tissue. ATMs in formerly obese mice demonstrated a proinflammatory profile, including elevated expression of interferon-γ, tumor necrosis factor-α, and interleukin-1β. T-cell–deficient Rag1$^{-/-}$ mice showed a degree of ATM persistence similar to that in WT mice, but with reduced inflammatory gene expression. ATM proliferation was identified as the predominant mechanism by which ATMs are retained in adipose tissue with WL. Our study suggests that WL does not completely resolve obesity-induced ATM activation, which may contribute to the persistent adipose tissue damage and reduced insulin sensitivity observed in formerly obese mice.

Obesity induces a state of chronic, low-grade inflammation characterized by qualitative and quantitative changes in the leukocytes of metabolic tissues including the hypothalamus, liver, and adipose tissue (1–3). In particular, inflammation within visceral adipose tissue (AT) of obese mice and humans has been shown to be associated with diabetes and to contribute to the development of insulin resistance; multiple cellular sources contribute to the inflammatory environment, including adipocytes, stromal cells, and leukocytes (4,5). In mice, a proinflammatory CD11c$^+$ macrophage population accumulates in visceral AT during obesity and assumes a metabolically activated phenotype that is associated with the development of systemic insulin resistance (6–8). Recruitment of circulating bone marrow–derived monocytes as well as proliferation contribute to CD11c$^+$ AT macrophage (ATM) accumulation and maintenance (9–11). AT T-cell–dependent signals have also been shown to promote CD11c$^+$ ATM accumulation and inflammation with obesity (12,13).

While the understanding of how AT inflammation is generated with obesity is fairly detailed, relatively little is known regarding how AT leukocytes respond to weight loss (WL) following obesity. Previous studies have shown varying degrees of change in AT inflammation after WL through different regimens. Interventions such as caloric restriction or bariatric surgery can improve metabolic dysfunction and reduce markers of inflammation within AT (14–16). However, several studies suggest that WL may not fully resolve AT inflammation and insulin sensitivity. Inflammation-related gene expression in subcutaneous AT of formerly obese human subjects remains high compared with expression in lean individuals (17,18). Similar results

[1]Graduate Program in Immunology, University of Michigan Medical School, Ann Arbor, MI
[2]College of Literature Sciences and Arts, University of Michigan, Ann Arbor, MI
[3]Soonchunhyang Institute of Medi-bio Science, Soonchunhyang University, Cheonan-si, Chungcheongnam-do, Korea
[4]Department of Cellular and Molecular Biology, University of Michigan Medical School, Ann Arbor, MI
[5]Department of Pediatrics and Communicable Diseases, University of Michigan Medical School, Ann Arbor, MI

Corresponding author: Carey N. Lumeng, clumeng@umich.edu.

Received 19 April 2016 and accepted 29 October 2016.

have been observed in mice: WL has been shown to be associated with the persistent expression of inflammatory cytokines such as interleukin (IL)-6, IL-1β, and tumor necrosis factor (TNF)-α in AT (19–22). Schmitz et al. (21) recently demonstrated that WL improved glucose tolerance but incompletely resolved AT inflammation and insulin sensitivity in mice and humans. Few studies have specifically examined how WL influences the quantity and quality of AT leukocytes. Weight cycling in mice suggests that interferon (IFN)-γ–expressing T cells accrue during successive exposures to a high-fat diet (HFD), indicating an incomplete resolution of lymphocyte activation with WL (23). WL has also been shown to induce short-term ATM recruitment in response to lipolytic signals (24).

Understanding the cellular and molecular events that reshape AT leukocytes during the resolution of obesity may identify pathways that are important in promoting WL and improving insulin resistance. Therefore, our objective was to perform a detailed investigation of the effects of WL on inflammatory leukocyte activation and composition within AT to understand the mechanisms by which metainflammation may resolve. We found that WL improved glucose tolerance; however, abnormal insulin resistance persisted systemically and in visceral AT. This was associated with long-term alterations in the composition of AT leukocytes, including retention of proliferating CD11c$^+$ ATMs, expansion of AT lymphocytes, and persistent activation of ATMs despite WL. Understanding which inflammatory characteristics of obesity remain despite WL helps inform our understanding of the relationship between AT inflammation and metabolic function.

RESEARCH DESIGN AND METHODS

Animals and Animal Care
Male Rag1$^{-/-}$ (B6.129S7-Rag1tm1Mom/J) and C57BL/6J mice were purchased from The Jackson Laboratory. Mice, at 6 weeks of age, were started on a normal (control) diet (ND; 4.09 kcal/g; 29.8% protein, 13.4% fat, 56.7% carbohydrate; PicoLab 5L0D; LabDiet) or an HFD (5.24 kcal/g; 20% protein, 60% fat, 20% carbohydrate; D12492; Research Diets Inc.).

Glucose tolerance tests (GTTs) and insulin tolerance tests (ITTs) were performed after 6 h of fasting. Mice were injected i.p. with D-glucose (0.7 g/kg) for GTTs and human recombinant insulin (1 U/kg) for ITTs. Insulin and leptin were measured using ELISA (Crystal Chem Inc.). Energy metabolism was measured using Comprehensive Lab Animal Monitoring System analysis (Columbus Instruments International) and body composition using nuclear magnetic resonance (Minispec LF90II; Bruker Optics). All mice procedures were approved by the University of Michigan Committee on Use and Care of Animals and were conducted in compliance with the Institute of Laboratory Animal Research's Guide for the Care and Use of Laboratory Animals.

Isolation of AT Stromal Vascular Fraction and Flow Cytometry
Excised AT was digested in RPMI medium with 0.5% BSA and 1 mg/mL type II collagenase for 25min at 37°C, and the stromal vascular fraction (SVF) was separated from adipocytes by centrifugation. The following antibodies were used for flow cytometry: anti-CD45 (30-F11), anti-CD3e (145–2C11), anti-CD4 (GK1.5), anti-CD8a (53–6.7), anti-Foxp3 (FJK-16s), anti-IFN-γ (XMG1.2), anti-Ki67 (SolA15), anti-TNF-α (MP6-XT22), anti-CD40 (1C10), anti-CD80 (16–10A1), anti-CD86 (GL1), and anti-CD11c (N418) (eBioscience), and anti-IL-6 (MP5–20F3) and CD64 (X54–5/7.1) (BD Pharmingen; BD Biosciences). Analysis was performed on a BD FACSCanto II system and sorting was performed on a FACSAria III (BD Biosciences).

Gene Expression Analysis and Microarray
RNA was extracted from adipose using Trizol LS (Life Technologies) and cDNA was generated using a High-Capacity cDNA Reverse Transcription Kit (Applied Biosystems). SYBR Green PCR Master Mix (Applied Biosystems) and the StepOnePlus System (Applied Biosystems) were used for real-time quantitative PCR. *Gapdh* expression was used as an internal control for data normalization. Samples were assayed in duplicate, and relative expression was determined using the $2^{-\Delta\Delta}$ CT method. For microarray experiments, analysis was done using a Mouse Gene 2.1 ST plate and a WT Pico kit (Affymetrix, Santa Clara, CA). Expression values were calculated using a robust multiarray average. Data were filtered to remove probe sets with a variance less than 0.1 over all samples and then fit to a linear model (25,26). The false discovery rate was set at an adjusted P value of 0.05. Oligo_1.24.2 and limma_3.16.7 packages from Bioconductor were used for data analysis in the R statistical environment (R version 3.0.0).

Immunoblotting
AT was homogenized in radioimmunoprecipitation assay lysis buffer with phosphatase inhibitors (Roche). Protein concentration was determined using the Bio-Rad Protein Assay Dye Reagent. Proteins were labeled and visualized using an Odyssey infrared imaging system (LI-COR Biosciences). Antibodies used for immunoblotting included anti–peroxisome proliferator–activated receptor-γ (81B8), anti–insulin receptor substrate-1, anti–phospho-Akt (Ser473), anti-AKT, anti-adiponectin (C45B10), anti-caveolin (D46G3) (Cell Signaling Technology), and anti–β-actin (AC-40) (Sigma-Aldrich).

Glycerol Release, Collagen Quantification, and Cytokine Array
Release of glycerol was stimulated in minced 100-mg pieces of AT cultured for 5 h with or without isoproterenol (1 μmol/L), according to the manufacturer's instructions for the Glycerol Detection Kit for Explants (ZenBio). Explants were cultured in serum-free AIM V media with AlbuMax and BSA (Life Technologies). Additional samples were hydrolyzed in 6 mol/L HCl, according to manufacturer's

instructions for the Total Collagen Assay Kit (QuickZyme BioSciences). Culture supernatant glycerol and adipose hydroxyproline contents were measured using colorimetry. The Mouse Cytokine Antibody Array (R&D Systems) was used to evaluate cytokine output from AT explants after 48 h and pooled from 3 samples. Quantitation was performed using ImageJ software after subtracting the background and normalizing to reference controls.

Immunohistochemistry and Immunofluorescence

Ki67 immunohistochemistry and hematoxylin-eosin (H-E) staining were performed by the University of Michigan's Comprehensive Cancer Center Histology Core. A Picrosirius Red Stain Kit (Polysciences, Inc.) was used following the manufacturer's instructions. Antibodies used for immunofluorescence included polyclonal anticaveolin (BD Pharmingen; BD Biosciences) and anti-Mac2 (Galectin-3; eBioM3/38; eBioscience).

PKH26 Labeling of Macrophages In Vivo

A PKH26 Cell Linker Kit for phagocytic cell labeling (Sigma-Aldrich) was used for in vivo macrophage labeling experiments, per the manufacturer's instructions. Briefly, 500 μL of a 1 μmol/L solution of PKH26 dye mixed with a diluent was injected i.p. into two sets of mice (those fed an ND and those fed an HFD) before WL. The first set was euthanized 1 day later to check labeling efficiency, and the second set was euthanized after WL (8 weeks); PKH26 uptake was evaluated using flow cytometry.

Statistical Analyses

All values are reported as the mean ± SEM unless otherwise stated. Statistical significance of differences between ND controls and other diet groups were determined using the unpaired two-tailed Student t test or one-way ANOVA for multiple groups, with the Fisher least significant difference test for planned statistical comparisons to the ND group (unless otherwise noted) using GraphPad Prism V6.05.

RESULTS

Withdrawal of an HFD Decreases Adiposity and Improves Glucose Tolerance but Not Insulin Tolerance in Mice

We established a model of WL based on the withdrawal of the HFD. Male C57BL/6J mice were fed an HFD (60% kcal from fat) or an ND (13.5% kcal from fat) for 12 weeks. Obese mice were then either maintained on the HFD or switched to the ND to induce WL over a period of 2–24 weeks (Fig. 1A). After 8 weeks of the switched diet, body weight of mice that showed WL decreased ~28%, from 44.8 g (SD ±2.8 g) to 31.8 g (SD ±2.3 g), and was similar to WL in age-matched mice fed the ND (29.6 g [SD ±1.8 g]) (Fig. 1B). Body composition analysis showed no significant differences in the percentages of fat and lean mass between ND-fed mice and mice with WL (data not shown). Epididymal white AT (eWAT) and inguinal white AT (iWAT) masses and adipocyte size in eWAT normalized by 4 weeks off the HFD (Fig. 1C and D).

GTTs and ITTs were performed to assess metabolism after WL. After 8 weeks of WL, fasting glucose and glucose tolerance decreased to levels similar to those in ND-fed mice (Fig. 1E). Fasting serum insulin concentrations decreased but remained elevated compared with ND-fed controls (Fig. 1F). ITTs revealed improvement in insulin sensitivity in mice with WL compared with those fed the HFD, but insulin tolerance remained abnormal compared with ND-fed mice (Fig. 1F). Leptin levels were lower in mice with WL compared with those fed the HFD, but they remained elevated compared with the ND group (Fig. 1G). Food intake and energy expenditure increased in mice with WL compared with HFD-fed mice but remained lower than ND-fed controls (Fig. 1H and I). The respiratory exchange ratios for ND-fed mice and those with WL were not significantly different, and were higher in both groups than in HFD-fed mice. No differences in physical activity were noted between groups. Overall, these studies demonstrated that formerly obese mice retained persistent abnormalities in insulin sensitivity despite normalization of body weight, fat mass, and glucose tolerance.

### Measures of AT Dysfunction Persist Despite WL After HFD

We next evaluated whether AT structure normalized with WL concomitant with the normalization of depot mass. Crown-like structures (CLSs), a characteristic histologic feature of AT in obese mice, were induced with 12 weeks of an HFD. Despite WL, CLSs remained a prominent feature of eWAT and were similar in quantity to those in mice maintained on the HFD for 20 weeks (Fig. 2A). Picrosirius red staining demonstrated an association between the persistence of CLSs and AT fibrosis in mice with WL (Fig. 2B). Biochemical quantification of hydroxyproline content in AT supported this finding of increased fibrosis (Fig. 2C).

We next examined several measures of adipocyte function in mice with WL. To assess lipolysis, glycerol release from explants at baseline was examined and found to be similar between ND, 20-week HFD, and 8-week WL explants (Fig. 2D). Isoproterenol-stimulated glycerol release was decreased in HFD-fed mice compared with ND-fed mice and was restored after WL. Cytokine release was assessed in eWAT explants using cytokine arrays (Fig. 2E). AT secretion of CCL3, CCL4, CCL5, and CXCL9 was increased in eWAT of mice with WL compared with those fed the HFD. IL-1RA and CCL12 were increased in both HFD-fed mice and mice with WL compared with ND-fed mice.

Immunoblots demonstrated decreases in peroxisome proliferator–activated receptor-γ, insulin receptor substrate-1, and total Akt protein expression in eWAT from HFD-fed mice and mice with WL compared with the ND group (Fig. 2F and G). Caveolin and 27-kDa adiponectin were similar between groups. Adipose AKT serine 473 phosphorylation (pAKT) was decreased in HFD-fed mice and mice with WL at baseline (Fig. 2G and H), but pAKT in mice with WL was not significantly different from ND-fed mice after insulin
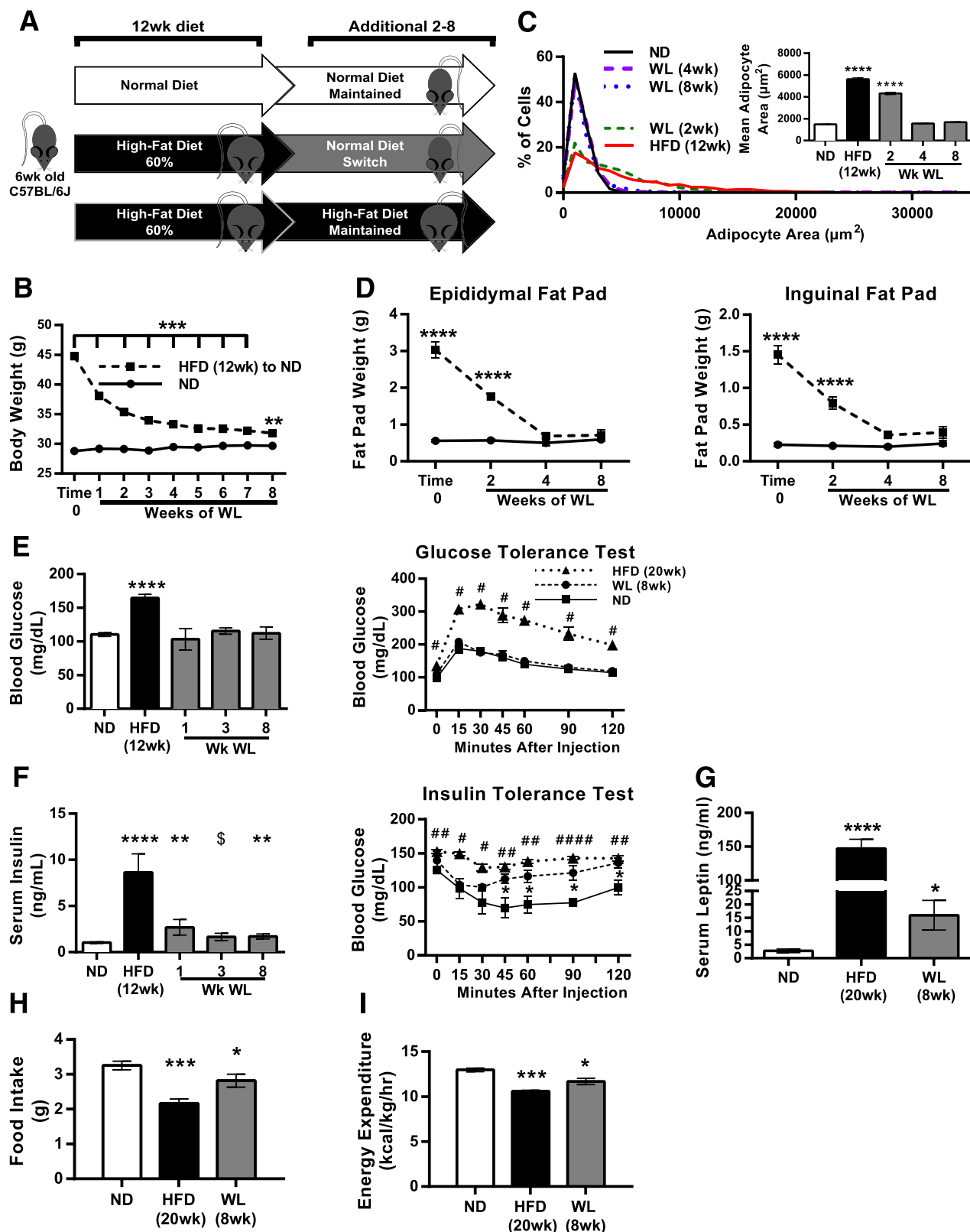
Figure 1—Glucose tolerance normalization but persistently elevated insulin with WL. *A*: Illustration showing obesity induction and the WL model. *B*: Body weight curve after WL (ND-fed mice, $n \geq 12$; mice with WL, $n \geq 16$). *C*: Adipocyte size distribution and average adipocyte size. *D*: Fat pad weight curve after WL ($n = 4$). *E*: Fasted blood glucose and glucose tolerance after WL ($n \geq 4$). #HFD vs. ND. *F*: Fasted serum insulin ($n \geq 4$) and insulin tolerance after WL ($n = 4$). #HFD vs. ND; $WL vs. ND. *G*: Fasted serum leptin concentrations ($n = 8$). *H* and *I*: Food intake measures (*H*) and energy expenditure (*I*) ($n = 4$). *$P < 0.05$, ## or **$P < 0.01$, ***$P < 0.001$, #### or ****$P < 0.0001$; significance compares with the ND-fed control group unless otherwise indicated.
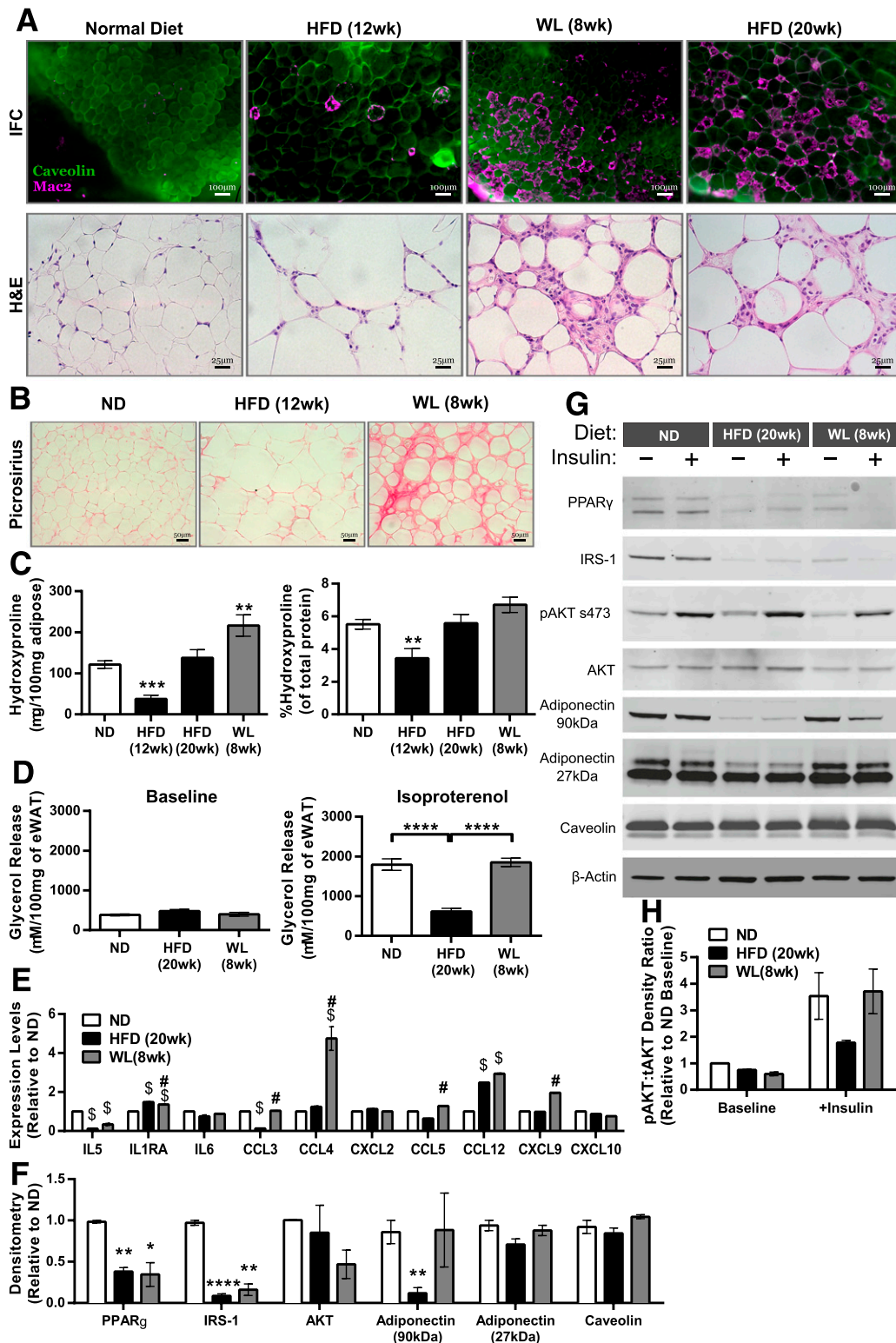
Figure 2—Epididymal AT maintains features associated with obesity despite WL. *A*: Immunofluorescence (IFC) and H-E–stained eWAT slides representing each diet condition, showing the development and maintenance of CLSs. *B*: Picrosirius red staining of eWAT slides representing diet conditions. *C*: Hydroxyproline quantification of eWAT ($n \geq 4$). *D*: Isoproterenol-stimulated glycerol release from whole eWAT explants ($n = 8$). *E*: eWAT explant multiplex cytokine array ($n = 2$ per condition). $P < 0.05$ vs. ND; #$P < 0.05$ vs. HFD. *F*: Quantification of densitometry measurements from immunoblots of whole eWAT (ND, $n = 2$; HFD, $n = 4$; WL, $n = 4$; ANOVA with Dunnett multiple comparisons). *G*: Representative immunoblots from mice injected i.p. with or without 1 U/kg insulin for 10 min, with two mice pooled per lane. *H*: Phosphorylated AKT s473 relative to total AKT (tAKT) from immunoblots ($n = 2$ for baseline; $n = 3$ for insulin administered). *$P < 0.05$; **$P < 0.01$; ***$P < 0.001$; ****$P < 0.0001$. Significance compares with the ND-fed control group unless otherwise indicated.

injection. Overall, these data demonstrate that formerly obese mice experience persistent derangements in AT architecture, fibrosis, adipogenic protein expression, and cytokine production.

ATMs Maintain a Proinflammatory Profile Despite WL

Flow cytometry was used to profile AT leukocyte changes with WL. The percentage of CD45$^+$ cells in the SVF of eWAT was increased with the HFD. Mice with WL had fewer CD45$^+$ leukocytes in the SVF than HFD-fed mice but remained increased compared with ND-fed mice, despite similar AT weights. ATMs (CD45$^+$, CD64$^+$ [27]) were reduced with WL but remained significantly elevated compared with ND-fed mice when expressed as either total ATMs per eWAT pad, ATMs per gram eWAT, or as a frequency of CD45$^+$ leukocytes (Fig. 3B–D). While total ATM content was reduced with WL, the frequency of CD11c$^+$ ATMs remained consistently elevated (Fig. 2E), indicating that formerly obese mice have long-term perturbations in ATM composition.

During obesity, CD11c$^+$ ATMs show a proinflammatory gene expression profile (7,28). To determine whether CD11c$^+$ ATMs from mice with WL retained proinflammatory characteristics, FACS-sorted ATMs were evaluated using gene expression microarrays. Microarrays revealed that all ATMs during obesity and after WL had similar gene expression profiles, regardless of CD11c (M1-like marker) or CD301 (M2-like marker) expression; they were thus combined for the subsequent analyses. Pathway analysis identified enrichment of genes involved in cytokine–cytokine receptor interaction (mmu04060) and the chemokine signaling pathway (mmu04062) in ATMs from mice with WL compared with ND-fed mice (29). ATMs in mice with WL maintained a proinflammatory expression profile compared with those in ND-fed mice, including increased *Il-1β*, *Il-6*, *Tnfα*, *Cxcl1*, *Ccl4*, *Ccl5*, *Ccl11*, and *Ccl12* (Fig. 3F). Intracellular cytokine labeling of nonstimulated ATMs verified increased IL-6 (Fig. 3G) and TNF-α (Fig. 3H) protein expression despite WL. Immunofluorescence localization of active IL-1β revealed enrichment surrounding CLSs in HFD-fed mice that was sustained after WL (Fig. 3I). Overall this demonstrates a persistence of proinflammatory ATMs in mice with WL and suggests that WL is insufficient to deactivate ATMs.

Physiologic and Immune Cell Perturbations in AT Persist as Long as 6 Months Off the HFD

To establish how long the effects of obesity might persist in AT after WL, we extended our WL model to 24 weeks off the HFD. Body weights in mice with 24 weeks of WL were 35.8 g (SD ±1.3 g) compared with HFD-fed mice at 60.8 g (SD ±4.3 g) and ND-fed mice at 32.8 g (SD ±1.2 g) (Fig. 4A), whereas eWAT weight completely normalized (Fig. 4B). Total ATMs and CD11c$^+$ ATM content remained significantly elevated compared with ND-fed mice and was comparable to that in mice with 8 weeks of WL (Fig. 4C and D). Overall the data indicate prolonged maintenance of leukocyte population changes induced by obesity despite WL. Immunofluorescence revealed continued maintenance of CLSs (Fig. 4F). However,

H-E staining revealed that these CLSs were surrounded by less dense collagen deposition than CLSs found in mice with 8 weeks of WL. Mice with 24 weeks of WL also no longer retained the abnormal systemic insulin responsiveness (Fig. 4E) observed in those with 8-week WL.

We next evaluated whether the degree of ATM persistence is dependent on the duration of HFD exposure before switching the diet. Mice were placed on the HFD for 6, 9, or 12 weeks before switching to the ND for 8 weeks. All HFD groups gained weight (6 weeks: 37.45 g [SD ±3.5 g]; 9 weeks: 38.6 g [SD ±3.6 g]; and ND: 23.67 g [SD ±0.9 g]), but groups fed the HFD for 6 and 9 weeks gained less than the mice on the 12-week HFD (46.6 ± 2.0 g) (Fig. 4G). After WL, eWAT weights among all HFD durations were similar to that in ND-fed controls (Fig. 4H). Total ATM content after WL was higher than that in age-matched ND-fed mice and increased with longer time spent on the HFD (Fig. 4I). CD11c$^+$ ATMs after WL in mice fed the HFD for 6 and 9 weeks remained slightly increased compared with ND-fed controls (Fig. 4J). However, mice fed the HFD for 12 weeks before WL had significantly more CD11c$^+$ ATMs after WL than the groups exposed to the HFD for shorter times. Immunofluorescence after WL revealed fewer CLSs in the mice fed the HFD for 6 and 9 weeks (Fig. 4K) compared with those on the 12-week HFD (Fig. 2A). These data indicate that the degree to which ATMs and CD11c$^+$ ATMs persist in AT after WL is dependent on the duration of the HFD or the degree of adiposity before the WL intervention.

WL Does Not Alter ATMs in Inguinal AT and Improves Liver Steatosis

Subcutaneous iWAT was also evaluated to determine how this AT depot responds to WL. iWAT weights remained significantly elevated after WL compared with ND-fed mice (Fig. 5A). Mice with WL had fewer CD45$^+$ leukocytes in iWAT than HFD-fed mice, and the values were similar to those in the ND group (Fig. 5B). Total ATMs trended toward being increased in HFD-fed mice and mice with WL but were not significantly different from those in the ND group (Fig. 5C). The frequency of all ATMs and CD11c$^+$ ATMs were not increased in the HFD-fed or WL mice compared with the ND group (Fig. 5D and E). Histology revealed few or no CLSs and little or no fibrosis in iWAT of HFD-fed or WL mice (Fig. 5F). Overall the results indicate that immune infiltration to murine iWAT during obesity is blunted compared with eWAT and remains low with WL. Liver histology revealed that steatosis after 12 weeks of the HFD resolved in mice with WL (Fig. 5G).

Increased IFN-γ Production Potential of Adipose T Cells After WL

Cross-talk between macrophages and T cells is critical for the activation of both cell types in obesity (30,31). We evaluated costimulatory marker expression in eWAT ATMs from mice with WL. Gene expression from sorted ATMs revealed reduced *Cd40* expression with the HFD compared with ND-fed controls, which increased with WL (Fig. 6A). WL induced
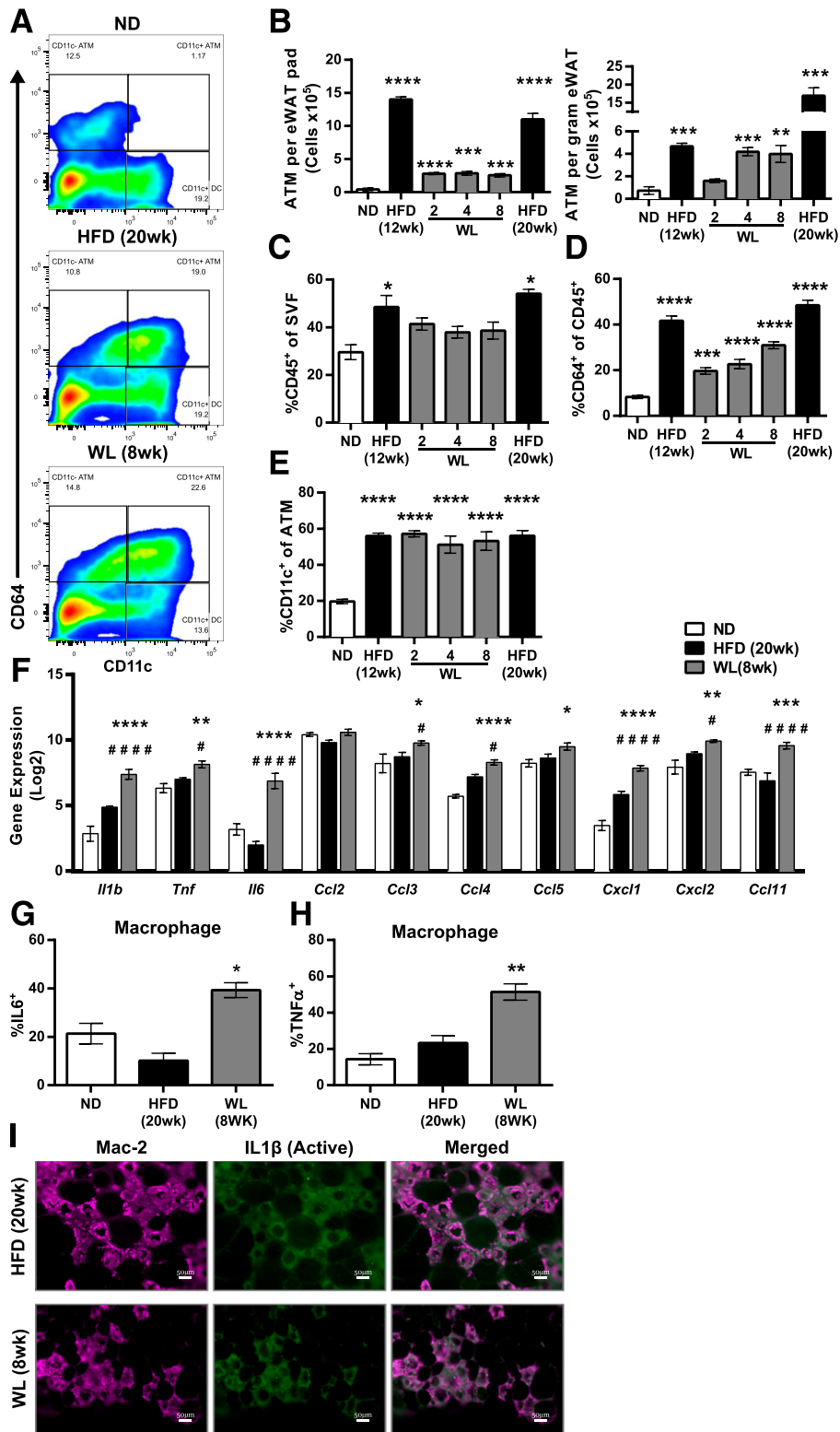
Figure 3—Maintenance of inflammatory CD11c^{+} ATMs despite WL. *A*: Representative flow plots showing our macrophage (CD45^{+}CD64^{+}) and dendritic cell (CD45^{+}CD64^{−}CD11c^{+}) gating strategy. *B*: Total ATM content per eWAT pad (left) and ATM content per gram of eWAT (right) ($n = 4$). *C*: Frequency of CD45^{+} immune cells among all eWAT SVFs ($n \geq 4$). *D*: Frequency of CD64^{+} ATMs among all CD45^{+} SVFs ($n \geq 4$). *E*: Frequency of CD11c^{+} ATMs among all CD45^{+}CD64^{+} ATMs ($n \geq 4$). *F*: Expression of select immune genes from microarrays of flow-sorted ATMs (two-way ANOVA with Dunnett multiple comparisons, $\alpha = 0.05$). #Significance compared with the WL to HFD groups. *G* and *H*: Intracellular cytokine staining of unstimulated SVF showing IL-6 protein expression (*G*) and TNF-α protein expression (*H*) from eWAT ATMs ($n = 4$). *I*: Immunofluorescence from eWAT showing cleaved IL-1β deposition surrounding CLSs in mice during obesity and after WL. Scale bars: 50 μm. *B–E*, *G*, and *H*, significance compared with the ND-fed control group. # or *$P < 0.05$; **$P < 0.01$; ***$P < 0.001$; #### or ****$P < 0.0001$. *Significance compares with ND; #significance compares with HFD.
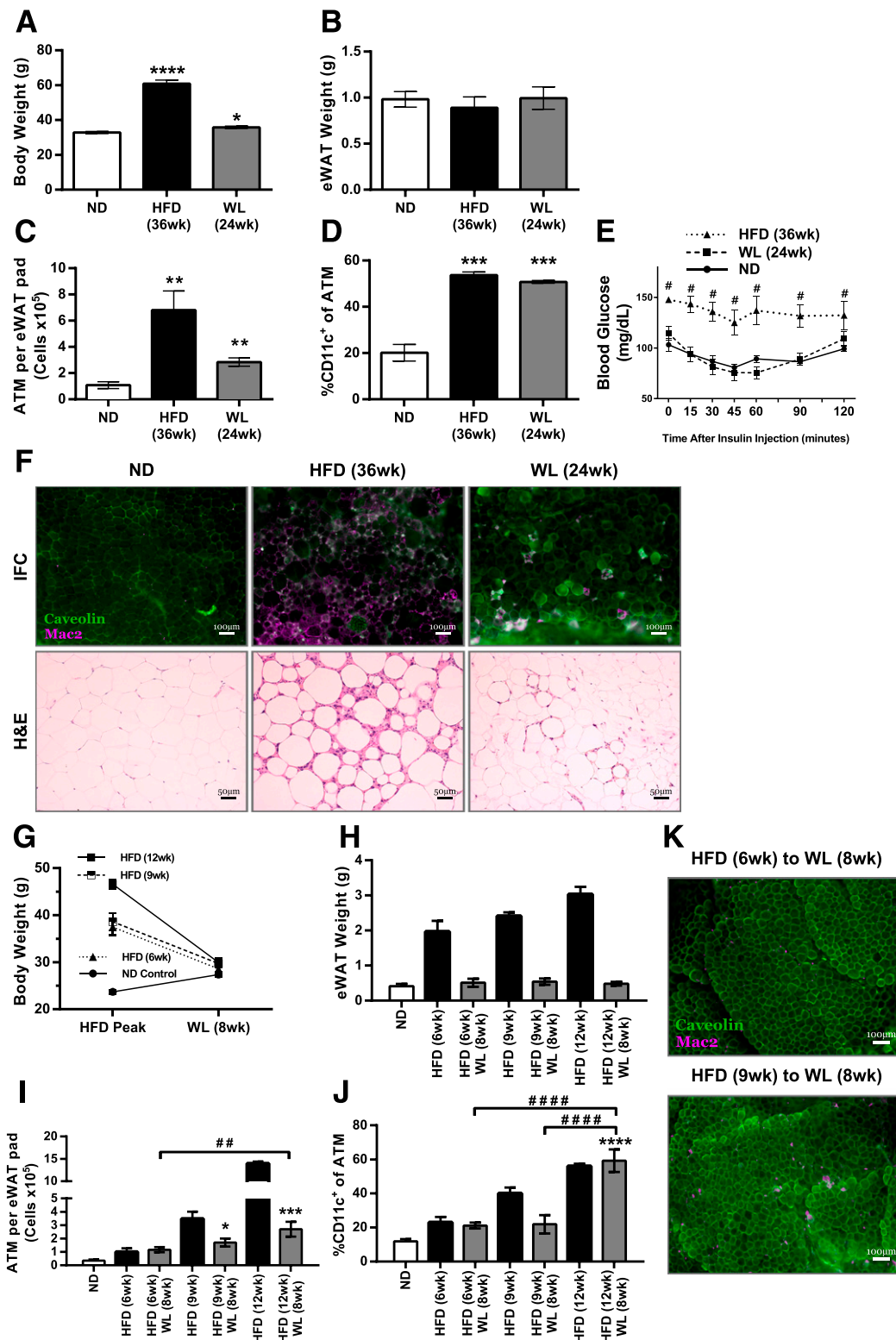
Figure 4—Obesity-induced effects can persist in AT as long as 6 months after removing the HFD. Body weight (*A*) and eWAT weight (*B*) of mice after 24 weeks of WL, along with those of respective controls (*n* = 4). *C*: Total CD45+CD64+ ATM content per eWAT for mice with 6 months of WL (*n* = 4 for all diet conditions). *D*: Frequency of CD11c+ ATMs among all CD45+CD64+ ATMs (*n* = 4). *E*: GTT results (*n* = 4). #*P* < 0.05; significance compares HFD with ND. *F*: Immunofluorescence (IFC) and H-E stained slides representing each diet condition, showing CLS development and maintenance. *G* and *H*: Body weight (*G*) and eWAT weight (*H*) after WL among mice in the 6-, 9-, or 12-week HFD feeding groups (*n* = 4 for all diet conditions). *I*: Total CD45+CD64+ ATM content per eWAT pad for mice fed the HFD for a short time (*n* = 4). *J*: Frequency of CD11c+ ATMs among all CD45+CD64+ ATMs (*n* = 4 for all diet conditions). *H–J*: ANOVA with Tukey multiple comparisons (α = 0.05) was used to compare WL averages to each other and to the ND-fed group. HFD points were not included in the analyses. *K*: Representative IFC images from eWAT showing macrophage accumulation. **P* < 0.05; ## or ***P* < 0.01; ****P* < 0.001; #### or *****P* < 0.0001. *Significance compares with ND; #significance between weight loss time points.
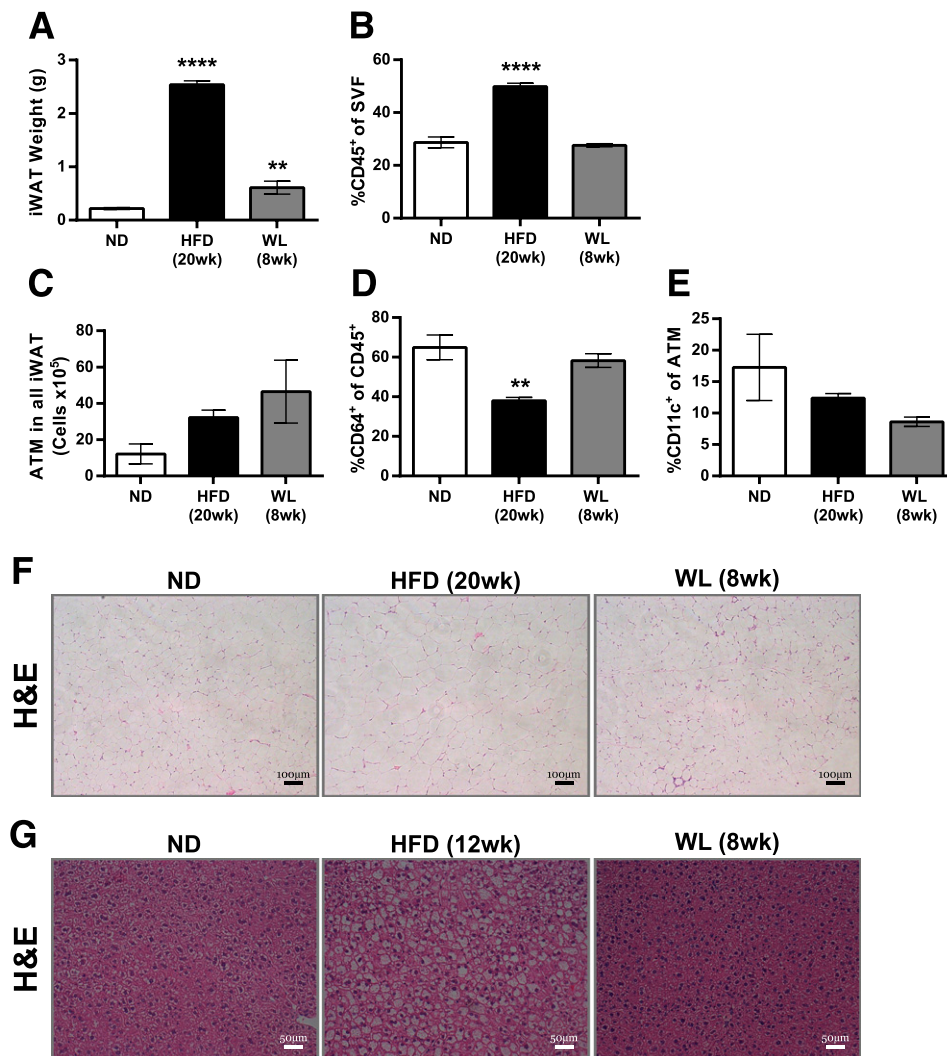
Figure 5—Inguinal AT and liver changes with WL. *A*: iWAT weights. *B*: Frequency of CD45$^+$ leukocytes among the total iWAT SVFs. *C*: Total CD45$^+$CD64$^+$ ATMs in iWAT. *D*: Frequency of ATMs among all CD45$^+$ iWAT SVF leukocytes. *E*: Frequency of CD11c$^+$ cells among all ATMs. $n = 4$ for *A*–*E*. *F* and *G*: H-E–stained iWAT (*F*) and (*G*) liver slides. **$P < 0.01$ and ****$P < 0.0001$. Significance compares with the ND-fed control group.

Cd80 expression in ATMs (Fig. 6*B*), whereas *Cd86* was reduced in ATMs of both HFD-fed mice and mice with WL compared with ND-fed controls (Fig. 6*C*). Surface expression of these markers was assessed using flow cytometry. CD40$^+$ and CD80$^+$ ATMs were significantly higher in mice with WL compared with ND-fed mice, whereas CD86$^+$ ATMs were elevated in both ND-fed and WL mice (Fig. 6*D*).

We next investigated how WL influenced AT T cells. Similar to ATMs, conventional CD4$^+$ T-cell and CD8$^+$ T-cell numbers increased with obesity (Fig. 6*E*). CD4$^+$ AT T cells decreased after 2 weeks and transiently increased 4 weeks after the diet was switched. CD8$^+$ AT T cells were decreased in mice with WL but remained significantly elevated compared with the ND-fed group up to 8 weeks after the diet was switched (Fig. 6*F*). Total Foxp3$^+$ regulatory AT T-cell numbers were also increased with obesity and returned to levels similar to those in ND-fed mice by 8 weeks of WL (Fig. 6*G*).

Type-1 polarization of T cells and IFN-γ has been implicated in obesity and insulin resistance (32–35). Evaluation of IFN-γ expression by flow cytometry demonstrated a reduction in the percentage of IFN-γ^+CD4$^+$ and IFN-γ^+CD8$^+$ AT T cells in HFD-fed compared with ND-fed mice (Fig. 6*H* and *I*). Decreased per-cell IFN-γ expression was also observed in obese mice. The frequency of IFN-γ^+CD4$^+$ AT T cells returned to the levels of those in the ND group after 2 weeks of WL. The frequency of IFN-γ^+ CD8$^+$ AT T cells returned to the levels of those in the ND group after 4 weeks of WL and was increased after 8 weeks. These data suggest that continued activation of CD4$^+$ and CD8$^+$ AT T cells occurs in AT in the setting of WL.

T Cells Contribute to ATM Activation With WL but Are Not Required for Macrophage Accumulation

Given the increase in AT T cells with WL, we evaluated whether T cells were required for the persistence of ATMs in formerly obese mice. T- and B-cell–deficient *Rag1*$^{-/-}$
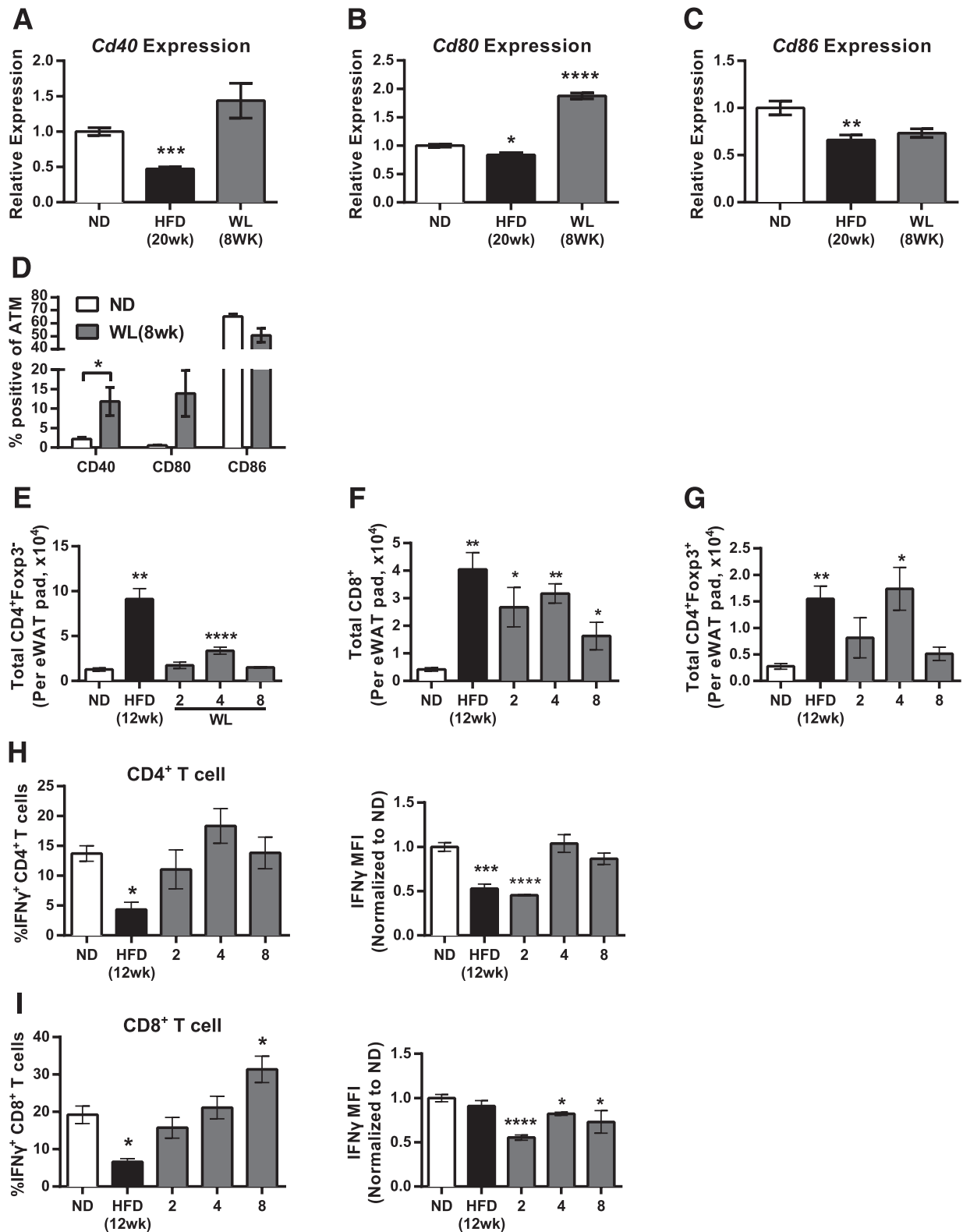
Figure 6—AT T-cell activation with WL. Quantitative RT-PCR from flow-sorted ATMs of mice evaluating *Cd40* (*A*), *Cd80* (*B*), and *Cd86* (*C*) gene expression (ATMs pooled from a total of 12 mice from the ND and HFD groups and 6 mice from the WL group; ND $n = 4$, HFD $n = 4$, WL $n = 2$). *D*: Surface marker expression of *Cd40*, *Cd80*, and *Cd86* evaluated by flow cytometry ($n = 4$). Total AT T-cell count per eWAT pad evaluated by flow cytometry for conventional CD4$^+$ T cells (*E*), CD8$^+$ T cells (*F*), and Foxp3$^+$CD4$^+$ T-regulatory cells (*G*) ($n \geq 4$ for *E*–*G*). *H* and *I*: Intracellular cytokine stain on phorbol myristic acetate/ionomycin stimulated the SVF to allow evaluation of IFN-γ production potential from CD4$^+$ T cells (*H*) and CD8$^+$ T cells (*I*). *$P < 0.05$; **$P < 0.01$; ***$P < 0.001$; ****$P < 0.0001$. Significance compares with the ND-fed control group. MFI, median fluorescence intensity.

mice and wild-type (WT) controls were fed the HFD for 12 weeks and then switched to the ND (Fig. 7A). $Rag1^{-/-}$ mice weighed less than WT mice before the diet was switched. Surprisingly, $Rag1^{-/-}$ mice with WL had significantly worse glucose tolerance compared with $Rag1^{-/-}$ ND-fed controls, despite similar body weights (Fig. 7B), which contrasts with the normalized GTTs of WT mice with WL (Fig. 1E). Similar to WT mice, $Rag1^{-/-}$ mice had significantly elevated total and CD11c$^+$ ATMs despite 8 weeks of WL (Fig. 7C and D). Histology demonstrated persistence of CLSs in WT and $Rag1^{-/-}$ mice with WL (Fig. 7H and I).

To evaluate the contribution of T and B cells toward ATM proinflammatory activity during WL, we assessed gene expression from flow-sorted ATMs in WT mice and $Rag1^{-/-}$ mice with WL. Il6, Tnfa, and Il1b were all significantly reduced in $Rag1^{-/-}$ mice with WL compared with WT mice with WL (Fig. 7E–G). $Rag1^{-/-}$ adipose insulin signaling was evaluated. Baseline phospho-AKT was decreased in $Rag1^{-/-}$ mice with WL but, similar to WT mice, was not significantly different from ND-fed mice after insulin injection (Fig. 7J). Taken together, the data show that T cells are not essential for the maintenance of CD11c$^+$ ATMs or the continual development of adipose fibrosis with WL in WT mice. However, signals from lymphocytes seem to contribute to the ongoing activation of ATMs in formerly obese mice.

After WL, ATMs Are Derived Primarily From Macrophages Present During Obesity and Maintained Through Proliferation

We next examined the mechanisms responsible for ATM persistence during WL. To determine whether recruitment was a significant contributor to ATM maintenance during WL, we used PKH26 pulse-labeling in ND- and HFD-fed mice before switching the diet. This method labels tissue macrophages but not blood monocytes, allowing identification of recruited ATMs as PKH26$^-$ cells (28). Mice fed the HFD for 12 weeks and the ND-fed controls were injected i.p. with PKH26. Labeling efficiency of ATMs assessed 1 day after PKH26 injection was similar in lean and obese mice (Fig. 8A and B). The frequency of PKH26$^+$ ATMs was examined after 8 weeks and was lower in ND-fed mice compared with the HFD or WL groups, demonstrating a higher rate of ATM retention in HFD-fed mice and mice with WL (Fig. 8C). The data indicate that new monocyte recruitment may not be the primary mechanism for the maintenance of CD11c$^+$ ATMs during WL.

Reduced apoptosis was also considered a potential mechanism of ATM maintenance. Annexin V labeling of ATMs was significantly reduced in HFD-fed mice and after 1 week of the switched diet compared with ND-fed mice, indicating these ATMs had a relatively low level of apoptosis, which may contribute to ATM maintenance in HFD-fed mice and mice with WL (Fig. 8D). This is surprising given the reduction in total ATM content observed during the early stages of WL (Fig. 3D) and suggests that ATM exfiltration may be responsible for the decrease.

Another mechanism for how ATMs may be retained without continual recruitment is proliferation. We evaluated ATM proliferation by Ki67 expression. Immunohistochemistry demonstrated an increase in Ki67$^+$ nuclei surrounding CLSs in mice with 8 weeks of WL compared with mice fed the HFD for 12 weeks and was comparable to that in mice fed the HFD for 20 weeks (Fig. 8E and F), suggesting a continual increase in proliferating cells despite WL. Flow cytometry demonstrated that >90% of the Ki67$^+$ cells in the SVF were CD45$^+$ leukocytes (Fig. 8G). ATMs made up >50% of these Ki67$^+$ SVF cells in both HFD-fed and WL mice, and both were significantly elevated compared with ND-fed controls (Fig. 8H). The overall frequency of Ki67$^+$ ATMs in HFD-fed and WL mice was also significantly higher than in the ND group (Fig. 8I). In addition, the frequency of Ki67$^+$CD11c$^+$ ATMs in HFD-fed and WL mice was significantly elevated compared with Ki67$^+$CD11c$^-$ ATMs (Fig. 8J). Taken together, the data indicate that CD11c$^+$ ATM maintenance during WL may primarily be the result of a combination of increased proliferation and reduced apoptosis.

DISCUSSION

In this study we used a mouse model of WL to understand leukocyte dynamics in AT of formerly obese mice. Our major finding is that chronic obesity leads to long-term alterations in AT leukocyte populations associated with persistent abnormalities in insulin tolerance that persist despite WL. Maintenance of CD11c$^+$ ATMs was observed as long as 6 months after the HFD was stopped. ATMs in mice with WL retained a proinflammatory profile, with elevated cytokine (IL-6, IL-1β, and TNF-α) and costimulatory marker expression. AT T cells were required for ATM activation, but were not required for sustaining ATMs in abdominal depots.

This persistent pattern of myeloid activation in AT with WL contrasts with tissue such as the hypothalamus, which shows a reversal of activation with the withdrawal of an HFD (36). ATMs were sustained in formerly obese mice primarily through local proliferation and decreased apoptosis, and not ongoing recruitment of blood monocytes. The mechanism for the induction and maintenance of ATM proliferation remains unclear at this time, but potential mechanisms include MCP-1 and IL-4 (10,37). The concentration of proliferating ATMs in CLSs suggests that lipid species may also regulate proliferation. Our findings are in agreement with those of other studies suggesting that WL only partially improves AT inflammation after it is established (19–22). The persistence and transient increase in CLSs is more robust than reported in other studies. One potential difference is our use of a 60% HFD for 12 weeks, a widely used model of chronic overnutrition (6,13,28,38,39). The leukocyte changes observed after removal of the HFD were dependent on the duration of HFD feeding. We have focused on the inflammatory activation of individual leukocyte subsets since few studies have compared the activation profiles of sorted ATMs after
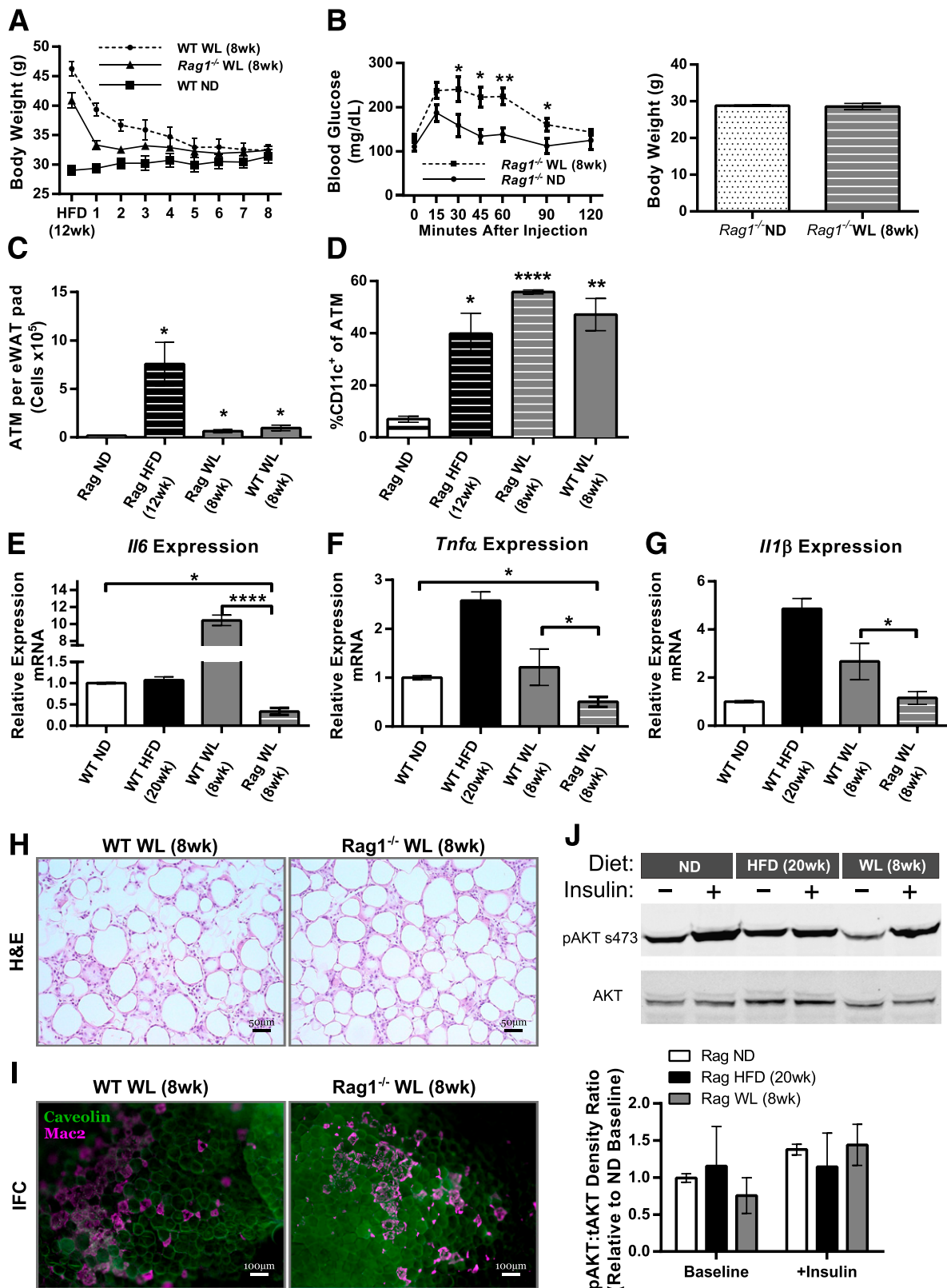
Figure 7—T cells are not required for CD11c⁺ macrophage accumulation but may control the inflammatory activation state. *A*: Body weight curves during WL (*n* ≥ 4). *B*: Glucose tolerance in *Rag1*⁻/⁻ knockout mice after WL (left) and normalization of total body weight (right) (*n* = 4). *C*: Total CD45⁺CD64⁺ ATM content per eWAT pad for *Rag1*⁻/⁻ mice (*n* ≥ 4). *D*: Frequency of CD11c⁺ ATMs among all CD45⁺CD64⁺ ATMs (*n* ≥ 4). Quantitative RT-PCR from flow-sorted ATMs evaluating *Il6* (*E*), *Tnfα* (*F*), and *Il1β* (*G*) gene expression (ATMs pooled from a total of 12 mice from the ND and HFD groups and 6 mice from the WL group; WT ND *n* = 4, WT HFD *n* = 4, WT WL *n* = 2, Rag WL *n* = 4). *H* and *I*: H-E stained slides (*H*) and representative immunofluorescence (IFC) images (*I*) showing CLS development and maintenance despite WL. tAKT, total AKT; +Insulin, insulin administered. *P* < 0.05; **P* < 0.01; ****P* < 0.0001. Significance compares with the ND-fed control group unless otherwise indicated.
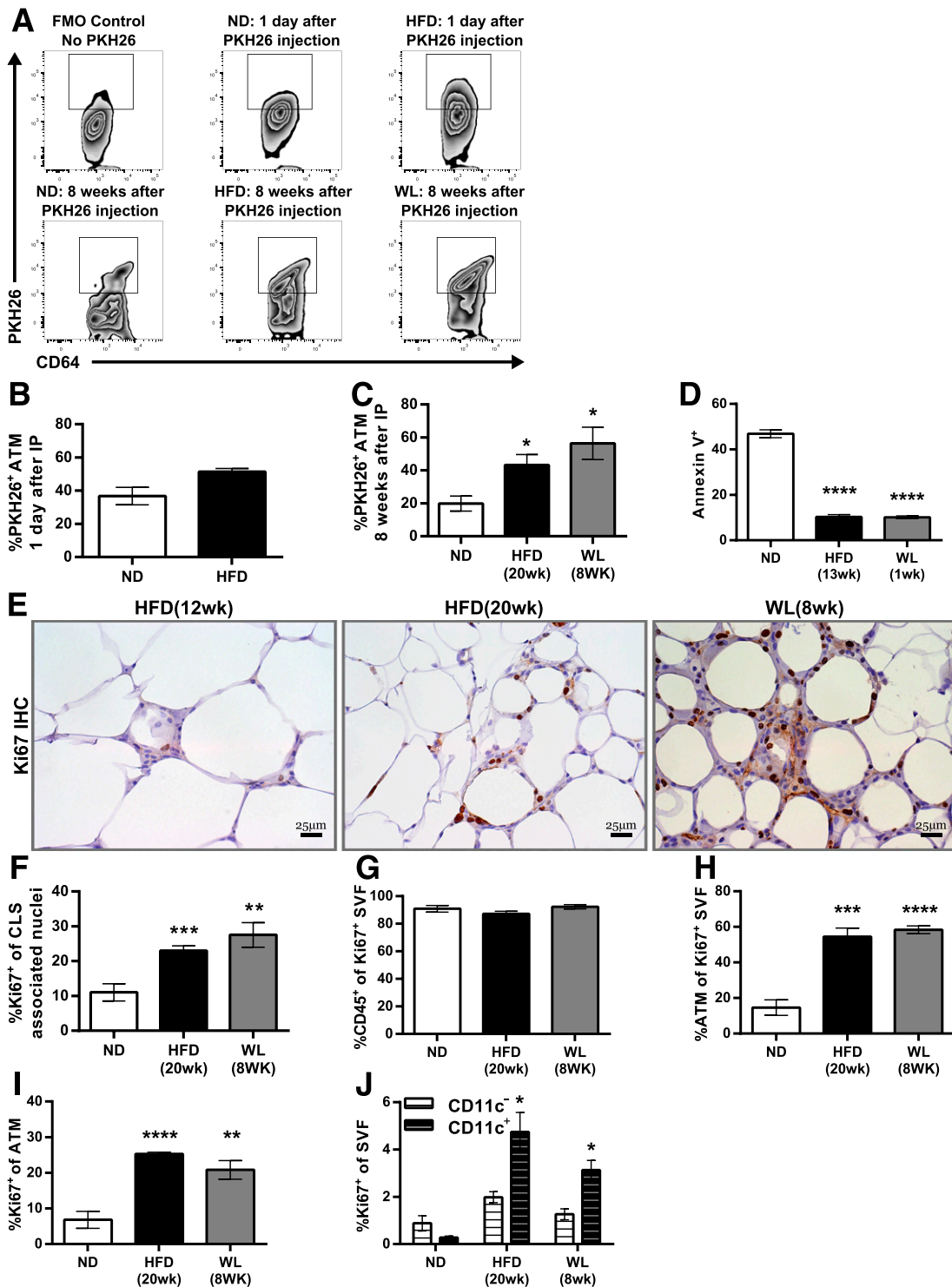
Figure 8—Macrophages are maintained through increased proliferation and reduced apoptosis. A: Representative flow cytometry plots gated on CD45$^+$CD64$^+$ ATMs showing PKH26$^+$ cells 1 day after injection, 8 weeks after injection, and a fluorescence minus one control (FMO) for PKH26. B and C: Frequency of PKH26$^+$ ATM either 1 day after injection (B) or 8 weeks after injection (C). D: Annexin V staining of SVFs as evaluated by flow cytometry (n = 4). E and F: Representative Ki67 immunohistochemistry (IHC) slides (E) and quantification of Ki67$^+$ nuclei surrounding CLSs from the immunohistochemistry images (F) (n ≥ 7). G: Frequency of CD45$^+$ immune cells among all Ki67$^+$ SVFs (n = 4). H: Frequency of ATMs among all Ki67$^+$ cells (n = 4). I: Frequency of Ki67$^+$ cells among all ATMs (n = 4). J: Frequency of Ki67$^+$ CD11c$^-$ (white) or Ki67$^+$ CD11c$^+$ (black) ATMs as a percentage of the entire SVF (n = 4). *P < 0.05; **P < 0.01; ***P < 0.001; ****P < 0.0001. Significance compares with the ND-fed control group except in J. Significance values for J compare CD11c$^+$ with CD11c$^-$.

WL. We observed reduced *Tnfα* and *Il1β* in WL ATMs compared with maintained HFD feeding, in agreement with other observations (6). However, *Il6* expression was substantially increased, and we found that the overall expression of inflammatory cytokines and chemokines remained significantly elevated in mice with WL compared with ND-fed mice.

Clinical studies have found persistent subcutaneous adipose inflammation after WL despite improvements in insulin sensitivity (17,19,21,40). Our observations are consistent with a growing literature that suggests a broader role for AT leukocyte activation. Thermoneutrality, for example, potentiates AT inflammation and ATM accumulation without abnormalities in glucose regulation (41). Low-level adipose inflammation is important for maintaining metabolic homeostasis (39). Overall, the literature indicates that the role played by AT inflammation is complex, with both detrimental and potentially beneficial effects on AT function.

We observed a persistent decrease in systemic and AT insulin sensitivity in WL mice; this was associated with architectural changes, more ATM content, and fibrosis, in agreement with other recent studies (6,17,21). Several proteins involved in adipocyte differentiation and insulin signaling were substantially reduced in formerly obese mice, despite a return to normal weight. Interestingly, the 24-week WL experiment shows that adipose fibrosis can be cleared with time. It is worth speculating that the retained ATMs may have beneficial functions related to resolving the excess extracellular matrix deposition, consistent with the role macrophages play in wound healing and matrix remodeling (42,43).

Given the connection between antigen-presenting cells and T-cell activation in AT, we evaluated T-cell changes with WL (31,34,35). Weight cycling was shown to alter T-cell composition in AT (23), and we observed dynamic changes in AT T cells in our model as well. IFN-γ^+ T cells, particularly CD8$^+$ T cells, were retained during WL. However, experiments in *Rag1*$^{-/-}$ mice revealed that T cells were not required for CD11c$^+$ ATM recruitment and maintenance. After WL, *Rag1*$^{-/-}$ mice remained glucose intolerant, which may relate either to ongoing adipose tissue inflammation caused by a lack of regulatory T cells (13), or to dysfunction in other metabolic tissues such as islets or the liver. Our findings instead indicate that local lymphocyte signals are necessary for the inflammatory activation of ATMs. This suggests lymphocyte stimulatory signals (i.e., CD40L or IFN-γ) could be targeted to attenuate inflammation while still preserving beneficial ATM functions.

Clinical studies have shown a persistent risk for cardiometabolic disease in formerly obese adults (17,21,45). Our study suggests that obesity elicits damage responses in AT that persist despite WL and that may contribute to this risk. We posit that maintenance of these features within AT, particularly inflammation, could contribute to the persistence of metabolic disease risk observed in formerly obese patients. It will be critical to compare our results using dietary manipulation with the induction of WL by other mechanisms such as bariatric surgery, which may impart different outputs in the inflammatory state of AT (45). A potential weaknesses of this study is that our WL protocol did not use isocaloric diets and did not control for food intake by pair feeding. It is possible that caloric restriction while maintaining an HFD to induce WL may provide different results. Our paradigm was designed to mimic current WL strategies that use reduced-calorie meal replacement to achieve WL. Future work will continue to investigate the physiologic consequences of these maintained features and whether the CD11c$^+$ ATM pool has potentially beneficial functions that could be separated from their deleterious effects.

References

1. Lumeng CN, Saltiel AR. Inflammatory links between obesity and metabolic disease. J Clin Invest 2011;121:2111–2117

2. Thaler JP, Yi CX, Schur EA, et al. Obesity is associated with hypothalamic injury in rodents and humans. J Clin Invest 2012;122:153–162

3. Gregor MF, Hotamisligil GS. Inflammatory mechanisms in obesity. Annu Rev Immunol 2011;29:415–445

4. Xu H, Barnes GT, Yang Q, et al. Chronic inflammation in fat plays a crucial role in the development of obesity-related insulin resistance. J Clin Invest 2003; 112:1821–1830

5. Weisberg SP, McCann D, Desai M, Rosenbaum M, Leibel RL, Ferrante AW Jr. Obesity is associated with macrophage accumulation in adipose tissue. J Clin Invest 2003;112:1796–1808

6. Li P, Lu M, Nguyen MT, et al. Functional heterogeneity of CD11c-positive adipose tissue macrophages in diet-induced obese mice. J Biol Chem 2010;285: 15333–15345

7. Kratz M, Coats BR, Hisert KB, et al. Metabolic dysfunction drives a mechanistically distinct proinflammatory phenotype in adipose tissue macrophages. Cell Metab 2014;20:614–625

8. Xu X, Grijalva A, Skowronski A, van Eijk M, Serlie MJ, Ferrante AW Jr. Obesity activates a program of lysosomal-dependent lipid metabolism in adipose tissue macrophages independently of classic activation. Cell Metab 2013;18:816–830

9. Weisberg SP, Hunter D, Huber R, et al. CCR2 modulates inflammatory and metabolic effects of high-fat feeding. J Clin Invest 2006;116:115–124

10. Amano SU, Cohen JL, Vangala P, et al. Local proliferation of macrophages contributes to obesity-associated adipose tissue inflammation. Cell Metab 2014; 19:162–171

11. Kanda H, Tateya S, Tamori Y, et al. MCP-1 contributes to macrophage infiltration into adipose tissue, insulin resistance, and hepatic steatosis in obesity. J Clin Invest 2006;116:1494–1505

12. Nishimura S, Manabe I, Nagasaki M, et al. CD8+ effector T cells contribute to macrophage recruitment and adipose tissue inflammation in obesity. Nat Med 2009;15:914–920

13. Winer S, Chan Y, Paltser G, et al. Normalization of obesity-associated insulin resistance through immunotherapy. Nat Med 2009;15:921–929

14. Clément K, Viguerie N, Poitou C, et al. Weight loss regulates inflammation-related genes in white adipose tissue of obese subjects. FASEB J 2004;18:1657–1669

15. Steckhan N, Hohmann CD, Kessler C, Dobos G, Michalsen A, Cramer H. Effects of different dietary approaches on inflammatory markers in patients with metabolic syndrome: a systematic review and meta-analysis. Nutrition 2016;32:338–348

16. Franz MJ, Boucher JL, Rutten-Ramos S, VanWormer JJ. Lifestyle weight-loss intervention outcomes in overweight and obese adults with type 2 diabetes: a systematic review and meta-analysis of randomized clinical trials. J Acad Nutr Diet 2015;115:1447–1463

17. Cancello R, Zulian A, Gentilini D, et al. Permanence of molecular features of obesity in subcutaneous adipose tissue of ex-obese subjects. Int J Obes 2013;37: 867–873

18. Magkos F, Fraterrigo G, Yoshino J, et al. Effects of moderate and subsequent progressive weight loss on metabolic function and adipose tissue biology in humans with obesity. Cell Metab 2016;23:591–601

19. Jung DY, Ko HJ, Lichtman EI, et al. Short-term weight loss attenuates local tissue inflammation and improves insulin sensitivity without affecting adipose inflammation in obese mice. Am J Physiol Endocrinol Metab 2013;304:E964–E976

20. Miller RS, Becker KG, Prabhu V, Cooke DW. Adipocyte gene expression is altered in formerly obese mice and as a function of diet composition. J Nutr 2008;138:1033–1038

21. Schmitz J, Evers N, Awazawa M, et al. Obesogenic memory can confer long-term increases in adipose tissue but not liver inflammation and insulin resistance after weight loss. Mol Metab 2016;5:328–339

22. Kalupahana NS, Voy BH, Saxton AM, Moustaid-Moussa N. Energy-restricted high-fat diets only partially improve markers of systemic and adipose tissue inflammation. Obesity (Silver Spring) 2011;19:245–254

23. Anderson EK, Gutierrez DA, Kennedy A, Hasty AH. Weight cycling increases T-cell accumulation in adipose tissue and impairs systemic glucose tolerance. Diabetes 2013;62:3180–3188

24. Kosteli A, Sugaru E, Haemmerle G, et al. Weight loss and lipolysis promote a dynamic immune response in murine adipose tissue. J Clin Invest 2010;120: 3466–3479

25. Smyth GK. Linear models and empirical bayes methods for assessing differential expression in microarray experiments. Stat Appl Genet Mol Biol 2004;3: Article3

26. Irizarry RA, Hobbs B, Collin F, et al. Exploration, normalization, and summaries of high density oligonucleotide array probe level data. Biostatistics 2003; 4:249–264

27. Gautier EL, Shay T, Miller J, et al.; Immunological Genome Consortium. Gene-expression profiles and transcriptional regulatory pathways that underlie the identity and diversity of mouse tissue macrophages. Nat Immunol 2012;13: 1118–1128

28. Lumeng CN, Deyoung SM, Bodzin JL, Saltiel AR. Increased inflammatory properties of adipose tissue macrophages recruited during diet-induced obesity. Diabetes 2007;56:16–23

29. Huang W, Sherman BT, Lempicki RA. Systematic and integrative analysis of large gene lists using DAVID bioinformatics resources. Nat Protoc 2009;4:44–57

30. Cho KW, Morris DL, DelProposto JL, et al. An MHC II-dependent activation loop between adipose tissue macrophages and CD4+ T cells controls obesity-induced inflammation. Cell Reports 2014;9:605–617

31. Morris DL, Oatmen KE, Mergian TA, et al. CD40 promotes MHC class II expression on adipose tissue macrophages and regulates adipose tissue CD4+ T cells with obesity. J Leukoc Biol 2016;99:1107–1119

32. O'Rourke RW, White AE, Metcalf MD, et al. Systemic inflammation and insulin sensitivity in obese IFN-γ knockout mice. Metabolism 2012;61:1152–1161

33. Mito N, Hosoda T, Kato C, Sato K. Change of cytokine balance in diet-induced obese mice. Metabolism 2000;49:1295–1300

34. Rocha VZ, Folco EJ, Sukhova G, et al. Interferon-gamma, a Th1 cytokine, regulates fat inflammation: a role for adaptive immunity in obesity. Circ Res 2008;103:467–476

35. Strissel KJ, DeFuria J, Shaul ME, Bennett G, Greenberg AS, Obin MS. T-cell recruitment and Th1 polarization in adipose tissue during diet-induced obesity in C57BL/6 mice. Obesity (Silver Spring) 2010;18:1918–1925

36. Berkseth KE, Guyenet SJ, Melhorn SJ, et al. Hypothalamic gliosis associated with high-fat diet feeding is reversible in mice: a combined immunohistochemical and magnetic resonance imaging study. Endocrinology 2014;155:2858–2867

37. Jenkins SJ, Ruckerl D, Thomas GD, et al. IL-4 directly signals tissue-resident macrophages to proliferate beyond homeostatic levels controlled by CSF-1. J Exp Med 2013;210:2477–2491

38. Buettner R, Schölmerich J, Bollheimer LC. High-fat diets: modeling the metabolic disorders of human obesity in rodents. Obesity (Silver Spring) 2007;15: 798–808

39. Wernstedt Asterholm I, Tao C, Morley TS, et al. Adipocyte inflammation is essential for healthy adipose tissue expansion and remodeling. Cell Metab 2014; 20:103–118

40. Divoux A, Tordjman J, Lacasa D, et al. Fibrosis in human adipose tissue: composition, distribution, and link with lipid metabolism and fat mass loss. Diabetes 2010;59:2817–2825

41. Tian XY, Ganeshan K, Hong C, et al. Thermoneutral housing accelerates metabolic inflammation to potentiate atherosclerosis but not insulin resistance [published correction appears in Cell Metab 2016;23:386]. Cell Metab 2016;23: 165–178

42. Chavey C, Mari B, Monthouel MN, et al. Matrix metalloproteinases are differentially expressed in adipose tissue during obesity and modulate adipocyte differentiation. J Biol Chem 2003;278:11888–11896

43. Bourlier V, Zakaroff-Girard A, Miranville A, et al. Remodeling phenotype of human subcutaneous adipose tissue macrophages. Circulation 2008;117:806–815

44. Dutton GR, Lewis CE. The Look AHEAD Trial: Implications for Lifestyle Intervention in Type 2 Diabetes Mellitus. Prog Cardiovasc Dis 2015;58:69–75

45. Frikke-Schmidt H, O'Rourke RW, Lumeng CN, Sandoval DA, Seeley RJ. Does bariatric surgery improve adipose tissue function? Obes Rev 2016;17:795–809